

09.5

Extended flexible terahertz waveguide with low attenuation

© Z.Ch. Margushev¹, K.A. Bzheumikhov¹, M.M. Nazarov²

¹ Institute of Informatics and Regional Management Problems Kabardino-Balkar Scientific Center, Russian Academy of Sciences, Nalchik, Russia

² National Research Center „Kurchatov Institute“, Moscow, Russia
E-mail: zmargush@yandex.ru

Received March 16, 2023

Revised April 24, 2023

Accepted April 26, 2023

The possibility of fabricating a flexible extended terahertz waveguide with low losses, which has a hollow core and a reflective shell of eight polypropylene capillaries located in a common shell with an outer diameter of 7.5 mm, has been demonstrated. The transmittance of terahertz pulses with frequencies of 2.3–2.8 THz through a waveguide (including a bended one, $R_{bent} \sim 60$ cm) longer than 3 m with an attenuation of 5 dB/m has been experimentally confirmed.

Keywords: terahertz, waveguide, capillary, drag and draw technology, polypropylene, negative curvature.

DOI: 10.61011/TPL.2023.06.56382.19558

The submillimeter wavelength range of the electromagnetic spectrum has been studied extensively in recent decades [1]. The interest in it stems from the following facts: frequencies of long-wave crystal lattice vibrations are within this range [2]; high-power terahertz (THz) pulses carry a giant electric and magnetic field of a picosecond duration, which allows one to excite intraband transitions in semiconductors and heterostructures [3]; a number of obstructive materials are transparent in this range, making them applicable in the development of security systems and remote THz probing systems [4,5]. Although the THz range has promising applications, it still lags behind the adjacent microwave and IR spectral regions. One major issue in this field consists in the development of methods for transmission of THz radiation from a source to a detector. The transmission of these frequencies in free space is inefficient, since atmospheric water vapor is a strong absorber in this range. Therefore, low-loss flexible waveguides are highly requested. It is a fundamental issue with fabrication of efficient waveguides that most available materials possess substantial absorption in the THz range. A waveguide channel needs to be positioned in a gas medium without water vapor (e.g., dry air or nitrogen). In advanced designs, this channel has a metal [6], dielectric [7], or hybrid metal–dielectric [8] cladding. The cladding serves to confine radiation to the central core with the purpose of maximizing the fraction of the electromagnetic wave field within an air medium. Polymers transparent in the THz range, such as polyethylene, polytetrafluoroethylene, cyclo olefin copolymer (Zeonex, Topas), and polypropylene (PP) [9], are promising candidate materials for flexible waveguides; their absorption coefficient is $\alpha < 4 \text{ cm}^{-1}$ at frequencies $f < 2 \text{ THz}$. Technological aspects of fabrication, which are specified by the physicochemical and thermophysical properties of a material, are no less important than absorption. Thus, materials engineering, optical (waveguiding

mechanism), and technological factors need to be taken into account to fabricate an efficient THz waveguide.

Waveguides with a polymer cladding may be produced using the following methods: drilling [10], extrusion [11], „drag and draw“ [12], and 3D printing [13]. Each of them has its advantages and disadvantages. Since flexible waveguides with a length upward of 0.5 m are needed in practice, the efficiency of a fabrication technique consists in stabilizing the cross-sectional structure dimensions throughout a considerable length.

The majority of published data on fabrication and measurements correspond to short (5–20 cm) waveguides. One exception here is study [14], where low (0.34 dB/m) propagation losses in the subTHz range were reported for a teflon tube 3 m in length and 9 mm in diameter. However, a waveguide of this fairly large diameter is multimode and (without a special structural shell) has high bending losses; therefore, it is ill-suited for practical applications.

The design with a reflective cladding formed by a single layer of contacting cylindrical capillaries in a protective shell is an efficient one for waveguides with a hollow core. The concept of a negative curvature of the core–cladding boundary has been first introduced for IR waveguides of the indicated design [15], and it has been demonstrated that this curvature is the reason why optical losses decrease significantly. In the THz range, the same has been demonstrated using the example of PP waveguides with an eight-capillary cladding [12,16]. The measured field amplitude attenuation was 7–10 dB/m within the 2–3 THz interval for samples 20–30 cm in length.

Figure 1, *a* shows the schematic diagram of the cross section of an eight-capillary waveguide with its structural parameters indicated. The strategy for optimization of cross-sectional dimensions of this configuration has been examined in our study [12]. It was found that the ultimate transparency of an ideal structure is specified by radius

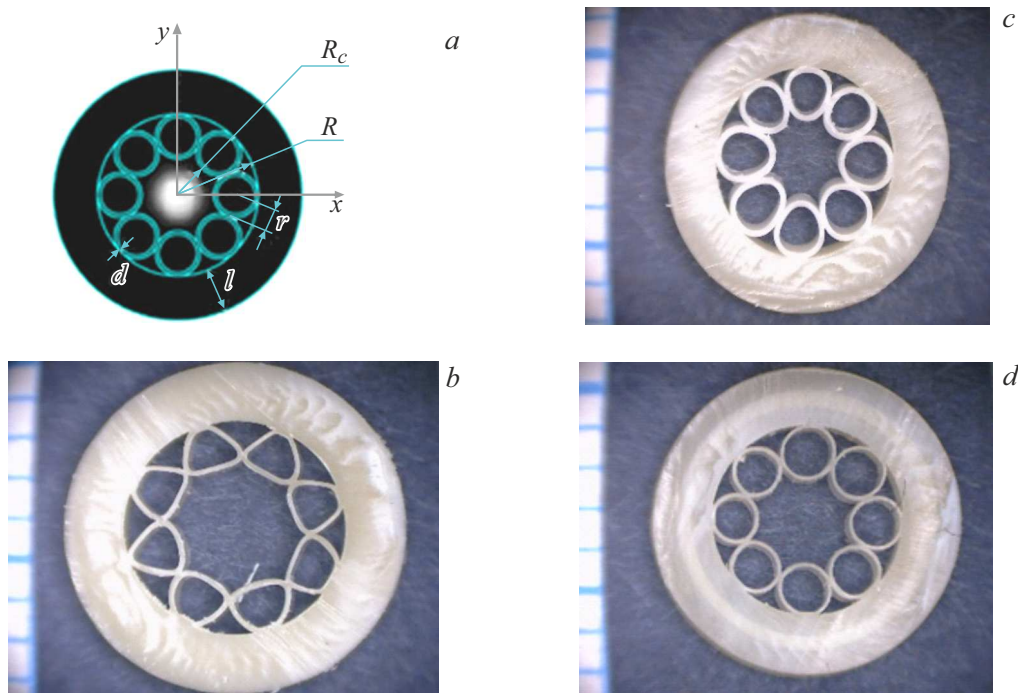


Figure 1. *a* — Schematic diagram of the cross section of a THz waveguide. R is the outer radius of the capillary cladding, R_c is the radius of the waveguide core, r is the outer radius of capillaries, d is the wall thickness of capillaries, and l is the thickness of the protective shell. The gray background at the center is the distribution of the field of the fundamental mode [5]. *b–d* — Photographic images of the cross section of experimental waveguides with a millimeter scale at the background.

R_c of the waveguide core, while the transparency ranges are set by thickness d of capillary walls. Radii R , R_c , and r for round undistorted capillaries are proportional to each other; the shape variation is specified, e.g., by ratio R/d . The transmission spectrum in this case contains a series ($i = 1, 2, 3, \dots$) of transparency windows at certain constant positions (d/λ_i) (see Fig. 2 in the present study and Fig. 2, *a* in [12]), and losses within these windows depend primarily on R/λ (see Fig. 3 in [12]), where λ is the wavelength. To achieve maximum transparency, one needs to maximize R/d and ensure that the shape and each dimension remain stable throughout the waveguide length. In practice, the R/d value depends on the fabrication technique; the growth of R is limited by the need to preserve flexibility and single-mode operation, while the reduction of d invokes the problem of uniformity of capillary walls that should be maintained to within several micrometers [16]. This study was focused on determining the optimum relation between transparency, flexibility, and performance features of the „stack and draw“ technique in order to achieve a sufficient stability of geometrical parameters on several-meter scales. The essence of this technique consists in fabricating a preform of the needed shape and a convenient scale, which is then reduced in size to the desired dimensions by heating and drawing performed in such a way that the preset proportions of the cross section are preserved. The task is not a trivial one and requires adjusting the heating temperature, the

rate of introduction (removal) of a preform into (from) a furnace, and the air pressure inside a preform. Only in a narrow range of these parameters are the accuracy and reproducibility of the cross-sectional structure maintained throughout the length of a sample [17]. Commercial PP tubes with an outer diameter of 25 mm and a wall thickness of 4.2 mm were used for experiments. Eight capillaries with an outer diameter of 4.5 mm and a length of 50 cm were first fabricated from them. The diameter was calculated so that all capillaries could be arranged tightly in a single-row ring along the inner wall of the initial tube. The preform was then drawn to the desired cross-sectional dimensions.

The aim was to fabricate a flexible waveguide that would have a better transmission and be 10 times longer (approximately 3 m) than the one examined in [12]. Values $R_c = 1000 \mu\text{m}$ and $d = 95 \mu\text{m}$ were set to maximize transparency at $\lambda \approx 120 \mu\text{m}$ while maintaining a sufficient flexibility; the corresponding waveguide diameter with the outer shell was ~ 7.5 mm. Three iterations *B*, *C*, and *D* corresponding to Figs. 1, *b–d* were needed to fabricate a sample with an undistorted cross section. The drawing process parameters were the same in all cases; the only variable parameter was the pressure at the central region of the waveguide, which was evacuated by a pump in the course of drawing. In the first case, air was not pumped out from the central cavity. It can be seen from Fig 1, *b* that capillaries got distorted so that the hollow core–cladding boundary became flat; i.e., negative curvature is

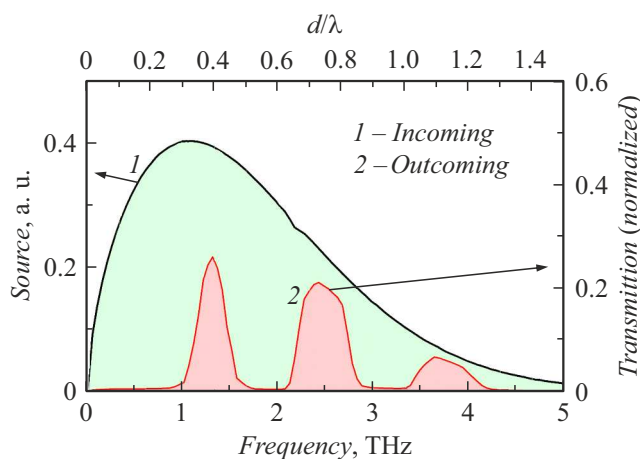


Figure 2. Incoming spectrum (normalized to unit area) (1) and calculated spectrum transmitted over 10 cm of waveguide D ($R_c = 1010 \mu\text{m}$, $d = 90 \mu\text{m}$) (2).

lacking. At the second stage, air was pumped out under a certain pressure from the central cavity of the preform. The corresponding Fig. 1, *c* shows that the pressure was too high, and capillaries became oval in shape (stretched toward the central point). At the third stage, an optimum pressure was set: the cross section of the waveguide had an undistorted shape (Fig. 1, *d*). The deviation of the outer diameter from 7.5 mm did not exceed 4% within the entire length (3 m) of all waveguides.

A high-power THz pulse source [18] based on a nonlinear LiNbO_3 crystal was used to measure the transmission of experimental waveguides. This crystal features a fine radiation resistance and a high electrooptical coefficient; it was specially fabricated to have a small thickness ($100 \mu\text{m}$) and a wide aperture of $40 \times 40 \text{ mm}$. After of LiNbO_3 , laser pumping radiation (250 mJ, 30 fs, 10 Hz, beam diameter: 2 cm) was extracted from the THz beam by a spectral splitter that reflected 98% of laser radiation and transmitted 80% of THz radiation. The remaining visible light was blocked by a black polyethylene filter, and THz radiation leaving the vacuum chamber through a silicon window was focused by a parabolic mirror with a focal distance of 5 cm to the waveguide entrance. The signal at the output edge was measured by a THz detector (Golay cell) by the amplitude of individual 10 Hz pulses recorded by an oscilloscope without any additional modulation. The measured signal is proportional to the energy of a THz pulse with wide spectrum. Each of the waveguides in Figs. 1, *b–d* was cut into two segments: a short segment (105 cm) and a long one (approximately 3 m). The transmission of short waveguides was measured as is, while long segments were bended into a ring $\sim 60 \text{ cm}$ in radius (the experimental setup was not suited to linear samples of this size).

The spectral characteristics are presented in Fig. 2. The incoming spectrum (curve 1) was obtained using a set of color filters [18]. Curve 2 corresponds to the calculated

spectrum transmitted over 10 cm of waveguide D . This curve was plotted based on the calculated universal d/λ and R/λ loss spectra, which were characterized in [12,16], with a 10% dispersion of waveguide dimensions taken into account. Three transparency windows are observed in the spectrum. In real-world structures, the second transparency window has the lowest attenuation and a sufficient width. The centers of transparency windows $f_i = c/\lambda_i$ ($d/\lambda_1 = 0.27$, $d/\lambda_2 = 0.74$, $d/\lambda_3 = 1.1$, ...) of all the fabricated structures coincide in the d/λ spectrum (the upper axis in Fig. 2). The second transparency band (specified by wall thickness d) of sample D corresponds to frequencies $f_2 = 2.3\text{--}2.8 \text{ THz}$ (the lower axis in Fig. 2), where the signal could be transmitted over several meters. The experimental signal is voltage amplitude S [mV] of a detector pulse. The magnitude of the input THz signal corresponding to a laser pulse energy of 250 mJ was $S_0 = 5000 \text{ mV}$ for all waveguides. The cross dimensions of samples corresponding to experimental data, optimum λ , ratios of physically significant quantities, and radiation losses are listed in the table. Theoretical losses were estimated based on R_c/λ_2 and calculations performed in [12]. Experimental losses were calculated as $\text{Loss} = -10 \lg(S/S_0)/L$ [dB/m]. The detector could not detect any signal at the output of waveguides shown in Figs. 1, *b, c* with lengths above 2 m. In calculations of the „transmission attenuation“ for the long bendet waveguide from Fig. 1, *d* ($L_1 = 314 \text{ cm}$, S_1 is the output signal), the input signal was taken from the output of the linear waveguide section ($L_2 = 105 \text{ cm}$, S_2 is the output signal) with entrance losses excluded: $\text{Loss} = -10 \lg(S_1/S_2)/(L_1 - L_2)$. The obtained value of 5 dB/m corresponds to an attenuation coefficient of $\alpha = 0.01 \text{ cm}^{-1}$. Note that low-loss transmission is feasible only within transparency bands (red area in Fig. 2; a color version of the figure is provided in the online version of the paper): in this case, these bands are centered at 1.4, 2.5, and 3.8 THz and have a width of $\sim 0.2 \text{ THz}$. It is also worth noting that the signal magnitude decreased by a factor of 4 when bend radius R_{bent} of sample D was reduced to 30 cm. Having compared the waveguides in the magnitude of $\delta d/d$, we found that optimum sample D has an almost two times higher spread than other samples; under otherwise equal conditions, the loss should have increased by 2–10% [16]. However, it turned out that transmission is affected in a greater extent by the shape of a hollow core (negative curvature): $\text{Loss}_D/\text{Loss}_B$. it is also evident that a maximum R_c value is not sufficient to reach the highest transparency. At the same time, the transparency of a structure with an ideal shape increases significantly with increasing ratios R_c/λ and R_c/d (see the column for theoretical losses; calculations were performed based on [12]). It also follows from the table that the overall attenuation per unit length of a short sample is two times higher than the attenuation for a long (and bendet) segment. This is attributable to high „spectral entrance losses“, since approximately 50% of the energy of a wideband pulse falling outside of the transparency bands (green area in Fig. 2) is attenuated completely even within a short segment.

Dimensions of samples and transmission losses for waveguides presented in Figs. 1, *b–d*

Sample	$L, \text{ cm}/R_{\text{bent}}, \text{ cm}$	$d \pm \delta d, \mu\text{m}$	$\lambda_2, \mu\text{m}$	$R_c, \mu\text{m}$	R_c/λ_2	Theoretical losses, dB/m	R_c/d	$S, \text{ mV}$	Measured losses, dB/m
<i>B</i>	105/ ∞	122 \pm 5	165	1330 \pm 20	8.0	0.7	10.8	27	22
<i>C</i>	105/ ∞	100 \pm 3	135	820 \pm 20	6	1.8	8.1	40	20
<i>D</i>	105/ ∞	90 \pm 5	122	1010 \pm 10	8.3	0.6	11.2	145	15
<i>D</i>	314/60	90 \pm 5	122	1010 \pm 10	8.3	0.6	11.2	12	5

Thus, the possibility of fabrication of a flexible THz waveguide with a length over 3 m, which, after being bent into a ring 60 cm in radius, transmits signals with an attenuation of approximately 5 dB/m within the 2.3–2.8 THz range, was demonstrated. This waveguide has a considerable advantage over the known alternatives in both length and frequency. The academic novelty of the study consists in estimation of the influence of deviation from the ideal shape of waveguides on their low attenuation. Short structures are not sensitive to such particularities. A comparison of three structures revealed the importance of negative curvature around the waveguide core and the value of R_c/d . Transmission characteristics may be improved significantly in further studies by suppressing the dimensional variation in the process of fabrication and removing water vapor from a waveguide.

Acknowledgments

The authors wish to thank D.A. Sidorov-Biryukov and V.V. Teplyakov for their help with measurements and A.B. Sotskii and A.V. Shilov for prior calculations.

Funding

This study was supported in part by the Ministry of Science and Higher Education of the Russian Federation under agreement No. 075-15-2022-830 dated May 27, 2022.

Conflict of interest

The authors declare that they have no conflict of interest.

References

- [1] D.M. Mittleman, *J. Appl. Phys.*, **122** (23), 230901 (2017). DOI: 10.1063/1.5007683
- [2] S.L. Dexheimer, *Terahertz spectroscopy: principles and applications* (CRC Press, Boca Raton, 2017).
- [3] R. Ulbricht, E. Hendry, J. Shan, T.F. Heinz, M. Bonn, *Rev. Mod. Phys.*, **83** (2), 543 (2011). DOI: 10.1103/RevModPhys.83.543
- [4] A.G. Davies, A.D. Burnett, W. Fan, E.H. Linfield, J.E. Cunningham, *Mater. Today*, **11** (3), 18 (2008). DOI: 10.1016/S1369-7021(08)70016-6
- [5] P.M. Solyankin, I.A. Nikolaeva, A.A. Angeluts, D.E. Shipilo, N.V. Minaev, N.A. Panov, A.V. Balakin, Y. Zhu, O.G. Kosareva, A.P. Shkurinov, *New J. Phys.*, **22** (1), 013039 (2020). DOI: 10.1088/1367-2630/ab60f3
- [6] K. Ito, T. Katagiri, Y. Matsuura, *J. Opt. Soc. Am. B*, **34** (1), 60 (2017). DOI: 10.1364/JOSAB.34.000060
- [7] A.S. Kucheryavenko, V.A. Zhelnov, D.G. Melikyants, N.V. Chernomyrdin, S.P. Lebedev, V.V. Bukin, S.V. Garnov, V.N. Kurlov, K.I. Zaytsev, G.M. Katyba, *Opt. Express*, **31** (8), 13366 (2023). DOI: 10.1364/OE.484650
- [8] H. Li, S. Atakaramians, R. Lwin, X. Tang, Z. Yu, A. Argyros, B.T. Kuhlmeier, *Optica*, **3** (9), 941 (2016). DOI: 10.1364/OPTICA.3.00094
- [9] M.S. Islam, C.M.B. Cordeiro, M.A.R. Franco, J. Sultana, A.L.S. Cruz, D. Abbott, *Opt. Express*, **28** (11), 16089 (2020). DOI: 10.1364/OE.389999
- [10] E. Arrospe, G. Durana, M. Azkune, G. Aldabaldetru, I. Bikandi, L. Ruiz-Rubioc, J. Zubiab, *Polym. Int.*, **67** (9), 1155 (2018). DOI: 10.1002/pi.5602
- [11] S. Atakaramians, S.V. Afshar, H. Ebendorff-Heidepriem, M. Nagel, B.M. Fischer, D. Abbot, T.M. Monro, *Opt. Express*, **17** (16), 14053 (2009). DOI: 10.1364/OE.17.014053
- [12] M.M. Nazarov, A.V. Shilov, K.A. Bzheumikhov, Z.Ch. Margushev, V.I. Sokolov, A.B. Sotsky, A.P. Shkurinov, *IEEE Trans. Terahertz Sci. Technol.*, **8** (2), 183 (2018). DOI: 10.1109/TTHZ.2017.2786030
- [13] L.D. Van Putten, J. Gorecki, E. Numkam Fokoua, V. Apostolopoulos, F. Poletti, *Appl. Opt.*, **57** (14), 3953 (2018). DOI: 10.1364/AO.57.003953
- [14] C.-H. Lai, Y.-C. Hsueh, H.-W. Chen, Y.-J. Huang, H.-C. Chang, C.-K. Sun, *Opt. Lett.*, **34** (21), 3457 (2009). DOI: 10.1364/OL.34.003457
- [15] A.D. Pryamikov, A.S. Biriukov, A.F. Kosolapov, V.G. Plotnichenko, S.L. Semjonov, E.M. Dianov, *Opt. Express*, **19** (2), 1441 (2011). DOI: 10.1364/OE.19.001441
- [16] M. Nazarov, A. Shilov, Z. Margushev, K. Bzheumikhov, I. Ozheredov, A. Angeluts, A. Sotsky, A. Shkurinov, *Appl. Phys. Lett.*, **113** (13), 131107 (2018). DOI: 10.1063/1.5040306
- [17] K.A. Bzheumikhov, Z.Ch. Margushev, Yu.V. Savoiskii, *J. Opt. Technol.*, **84** (2), 122 (2017) DOI: 10.1364/JOT.84.000122
- [18] M.M. Nazarov, P.A. Shcheglov, V.V. Teplyakov, M.V. Chashchin, A.V. Mitrofanov, D.A. Sidorov-Biryukov, V.Y. Panchenko, A.M. Zheltikov, *Opt. Lett.*, **46** (23), 5866 (2021). DOI: 10.1364/OL.434759

Translated by D.Safin